Detection of spin polarization with a side-coupled quantum dot

Tomohiro Otsuka,* Eisuke Abe, Yasuhiro Iye, and Shingo Katsumoto
Institute for Solid State Physics, University of Tokyo, 5-1-5 Kashiwanoha, Kashiwa, Chiba 277-8581, Japan
(Received 25 February 2009; revised manuscript received 22 April 2009; published 14 May 2009)

We propose realistic methods to detect local spin polarization, which utilize a quantum dot side coupled to the target system. By choosing appropriate states in the dot, we can put spin selectivity to the dot and detect spins in the target with small disturbance. We also present an experiment which realizes one of the proposed spin-detection schemes in magnetic fields.

DOI: 10.1103/PhysRevB.79.195313 PACS number(s): 73.63.Kv, 73.63.Nm, 72.25.Dc, 85.35.−p

I. INTRODUCTION

Electrical generation of electron-spin polarization in nonmagnetic semiconductors is a key technology in the development of spintronics.[1,2] The use of spin-orbit interaction[3–5] enables spin polarization without ferromagnets or external magnetic fields, and a variety of forms of spin filters based on the interaction have been proposed.[6–9] Although most of the proposed devices are technologically feasible, the main obstacle to the experimental verification lies in the detection part. A small ferromagnet attached to the outlet of a spin filter may be used as a polarization detector owing to its spin-dependent transparent coefficients. However, at the semiconductor-metal interface, the polarization generally suffers from conductance mismatch[10] and disorder-induced scattering, resulting in low-detection efficiency and strong disturbance to the spin source. It is also obvious that the use of ferromagnets is incompatible with the use of spin-orbit interaction. Therefore, polarization detectors that are made of the host material alone and "quiet" to the spin source are highly desired.

In this paper, we describe realistic methods to detect spin polarization by using a quantum dot (QD) tunnel coupled to a target (such as a spin filter). Since the dot and the target are connected at only a single point, our methods require no net current to flow through the dot, thus realizing a detector with extremely small disturbance to the target. These are suitable for the detection of spin polarization not only for delicate spin filters but also for spin-Hall effect.[11,12] Moreover, our methods are quite general and applicable to any system or material in which a few electron quantum dots can be prepared. As a proof of this principle, we present experiments on the polarization detection in magnetic fields utilizing a quantum wire (QW) as a controllable spin-polarization source.

II. DETECTION PRINCIPLE

Figure 1(a) shows the setup of the detector in which a QD is tunnel coupled to a target device via a single contact. The electrostatic potential of QD is detected through the conductance of a quantum point contact (QPC) placed on the other side of QD.[13–15] We first explain how the energy spectrum of QD (including excited states) is obtained in this device.[16,17] For the spectroscopy, the plunger gate voltage V_P on QD is driven to oscillate as a rectangular wave with the amplitude V_{amp} and the center voltage V_{Pc}, as illustrated in Fig. 1(b). V_P shifts the energy levels in QD up and down and induces shuttling of an electron between QD and the target. When the shuttling is forbidden, the electrostatic potential of QD simply follows the oscillation of V_P and thus the conductance through QPC results in a square wave in phase with V_P. When the shuttling has a finite probability, an electron injected into QD screens some portions of the variation of the electrostatic potential and diminishes the oscillation of the conductance. Then the shuttling is detected by the decrease in a lock-in signal g of the conductance through QPC in

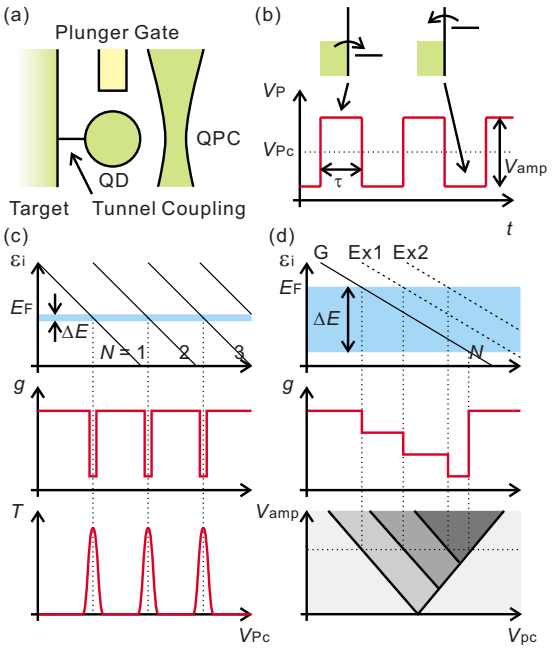

FIG. 1. (Color online) (a) Schematic of the proposed spin-polarization detector. (b) Waveform of V_P to perform energy spectroscopy in the side-coupled QD. Upper figures show the movement of an energy level in QD in phase with V_P. (c) Shift of ϵ_i (upper), schematic of g (middle), and Coulomb oscillations in the transmission probability T if we prepare a single electron-transistor structure (lower). The lines in the upper figure show the energy levels of $N=1$, 2, and 3 ground states from left to right. The energy window is indicated by the gray (blue) zone. (d) Shift of ϵ_i (upper), schematic of g with large V_{amp} (middle), and a gray scale plot of g as functions of V_{Pc} and V_{amp} (lower). The lines in the upper figure correspond to the energy of ground, first, and second excited levels of N-electron state from left to right.

phase with the applied square wave. From the diminishment of the lock-in signal Δg, the information on the energy levels in QD can be extracted.

An analytical approach tells that

$$\Delta g \propto 1 - \frac{\pi^2}{\Gamma^2\tau^2 + \pi^2}, \tag{1}$$

where Γ is the tunneling rate and τ is the half period of the square wave.[16] Γ is formally written as

$$\Gamma = \sum_{E_F - \Delta E < \epsilon_i < E_F} \gamma_i, \tag{2}$$

where i is the level index. γ_i and ϵ_i are the coupling constant and the energy level in QD at injection process (the period during $V_P = V_{Pc} + 1/2 V_{amp}$), respectively. E_F is Fermi energy of the target device and $\Delta E = e(C_g/C)V_{amp}$ is the width of the energy window in which the shuttling occurs. Levels satisfying $E_F - \Delta E < \epsilon_i < E_F$ cross E_F by the oscillation with V_{amp}. In the simplest case, γ_i is a common constant γ_0 and Γ becomes $N_{in}\gamma_0$, where N_{in} is the number of levels in the energy window. When V_{Pc} is swept, the energy levels in QD cross the energy window and Γ changes with the change in N_{in}. When ΔE is narrower than the energy-level spacing, N_{in} takes the value of 0 or 1 with the change in V_{Pc}. Then the energy levels in QD appear as a series of dips in g, the positions of which give the energy spectroscopy of the ground states in QD similar to the Coulomb oscillation [Fig. 1(c)]. If we increase V_{amp} and widen ΔE, N_{in} can be larger than 1. In this case, g should show stepwise decrease at which excited states come into the window as shown in Fig. 1(d). Hence the excitation energy spectra with fixed number of electrons in QD N can be obtained from the line shape of g versus V_{Pc} with a large V_{amp}. Here we assume that the dips are well separated, i.e., the charging energy is much larger than energy-level spacing between the excited states and multiple occupations of QD are forbidden.

Now we move onto the detection of spin polarization. Let $D_\uparrow$ and $D_\downarrow$ be the density of states at E_F for up and down spins, respectively. The spin polarization P is defined as $(D_\uparrow - D_\downarrow)/(D_\uparrow + D_\downarrow)$. To detect the polarization, we use two-electron state in QD. Due to the Pauli principle, the ground state is spin singlet and the excited state is spin triplet. A way for utilizing this property for polarization detection is to apply the sequence of V_P illustrated in Fig. 2(a). First, V_P is set in $N=0$ region and QD is emptied. Second, the first electron is injected and wait time τ_w. Finally, V_P is set between the singlet and triplet levels of $N=2$ state. When we make τ_w much longer than the spin-relaxation time T_1, the spin state of the first electron is not conserved and both spin states are realized with the probability of $\frac{1}{2}$. Then to form spin singlet, the tunneling rate of the second electron becomes

$$\Gamma = \frac{1}{2}AD_\uparrow + \frac{1}{2}AD_\downarrow = \frac{A}{2}(D_\uparrow + D_\downarrow) \equiv \Gamma_{nc},$$

where A is a constant. The first term represents the case in which the second electron has up spin and the second term shows the opposite case. On the other hand, when τ_w is much shorter than T_1, the spin state is conserved and the rate is

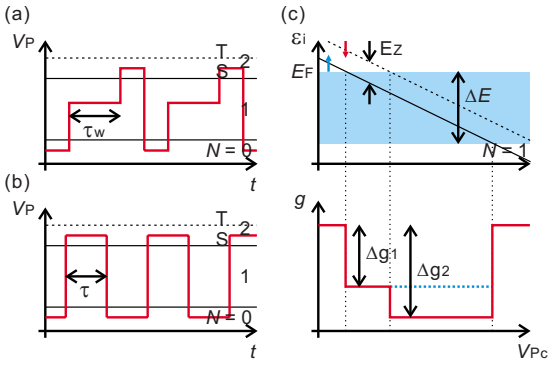

FIG. 2. (Color online) (a) Sequence of V_P to detect spin polarization. The horizontal lines show the energy levels of triplet and singlet of $N=2$ and $N=1$ states from top to bottom. (b) Another sequence of V_P to detect spin polarization. (c) Scheme of spin-polarization detection in high magnetic fields. Shift of ϵ_i (upper) and schematic of g (lower). The lines in the upper figure correspond to the energy levels of up and down spins of $N=1$ state from left to right. The dotted trace in the lower figure shows the result for $P=1$.

$$\Gamma = \frac{D_\downarrow}{D_\uparrow + D_\downarrow}AD_\uparrow + \frac{D_\uparrow}{D_\uparrow + D_\downarrow}AD_\downarrow = A\frac{2D_\uparrow D_\downarrow}{D_\uparrow + D_\downarrow} \equiv \Gamma_c,$$

which is equal to or less than Γ_{nc}. Now P can be obtained from the following relation:

$$\frac{\Delta\Gamma}{\Gamma_{nc}} \equiv \frac{\Gamma_{nc} - \Gamma_c}{\Gamma_{nc}} = \frac{(D_\uparrow - D_\downarrow)^2}{(D_\uparrow + D_\downarrow)^2} = P^2. \tag{3}$$

This equation allows us to evaluate P from the measurement of Γ.

In another method to detect the change in spin polarization, we utilize the square wave illustrated in Fig. 2(b). V_{amp} and V_{Pc} are adjusted, so that $N=1$ and the singlet level of $N=2$ states are contained in the energy window. At injection phase, two electrons can be injected into QD. The tunneling rate of the second electron is again given as

$$\Gamma = A\frac{2D_\uparrow D_\downarrow}{D_\uparrow + D_\downarrow}. \tag{4}$$

Here we assume that τ is much shorter than T_1. With the change in P, Γ is modified and this results in Δg. Especially if $P=1$ $(D_\downarrow = 0)$, it vanishes and the injection of the second electron is forbidden. With this technique we can confirm the change in P in spin filters which have controllability with external parameters.[8,18] The above two schemes work even in zero magnetic field.

Under the magnetic field, the detection becomes simpler. We again apply square wave on V_P. By applying magnetic field, the lowest level of $N=1$ state can accept only an up-spin electron due to the Zeeman energy E_Z as illustrated in Fig. 2(c). When only this state is in the energy window, the rate becomes $\Gamma = AD_\uparrow \equiv \Gamma_1$. With increasing V_{Pc}, the upper Zeeman state comes into the energy window and the rate changes to $\Gamma = A(D_\uparrow + D_\downarrow) \equiv \Gamma_2$. The ratio is thus

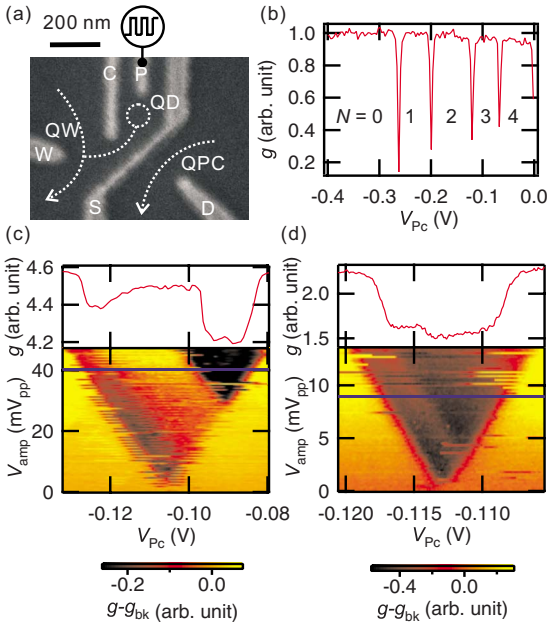

FIG. 3. (Color online) (a) Scanning electron micrograph of the device. White regions are Au/Ti gates deposited on the surface of a GaAs/AlGaAs wafer. (b) Measured g as a function of V_{Pc} with V_{amp}=4.5 mV and τ=1053 μs. (c) g as a function of V_{Pc} and V_{amp} with τ=680 μs (lower). In the graph, the background g_{bk} increasing with V_{amp} is subtracted for clarity. The upper graph shows the cross section along the solid line. (d) g as a function of V_{Pc} and V_{amp} (lower) and the cross section (upper). Magnetic field of 14 T is applied in parallel to the 2DEG.

$$\frac{\Gamma_1}{\Gamma_2} = \frac{D_\uparrow}{D_\uparrow + D_\downarrow} = \frac{1+P}{2} \tag{5}$$

which takes the value from 1/2 to 1. The former and the latter correspond to P=0 and P=1, respectively. Γ_1 and Γ_2 are obtained from the two depths Δg_1 and Δg_2 illustrated in Fig. 2(c). In this method, T_1 has no effect on the injection of an electron. In the following, we present experimental demonstration of this detection method.

III. EXPERIMENTAL DEMONSTRATION

Figure 3(a) shows a scanning electron micrograph of the device to realize the setup shown in Fig. 1(a). Au/Ti Schottky gates are deposited on a GaAs/AlGaAs heterostructure wafer containing two-dimensional electron gas (2DEG, depth: 60 nm, carrier density: 2.1×10^{15} m^{-2}, and mobility: 32 m^2/V s). By applying negative voltages on gates S, P, C and W, QD side coupled to a QW is formed. QW is the target of the spin-polarization detection in this setup. QPC is formed by gates S and D and acts as the detector of the electrostatic potential of QD. g is detected with lock-in measurement of the conductance through QPC in phase with the applied square wave on gate P. τ was set as 600 μs in almost all measurements. The device was cooled down to 30 mK by a dilution refrigerator and magnetic field up to 14 T in parallel to the 2DEG plane was applied by a superconducting solenoid.

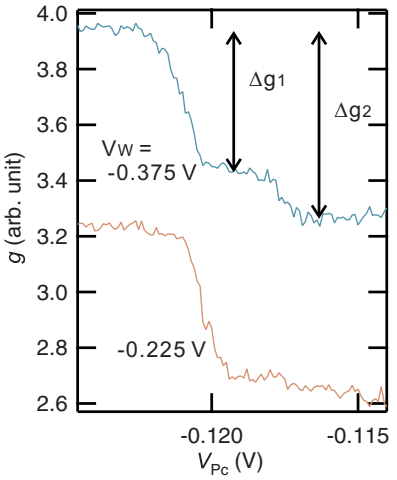

FIG. 4. (Color online) g as a function of V_{Pc}. The upper and lower traces are the results with V_W=−0.375 and −0.225 V, respectively. The upper trace has an offset of 0.7 for clarity.

In Figs. 3(b)–3(d), we review the energy spectrum measurement reported in Ref. 17. When V_{amp} is small, g versus V_{Pc} shows a series of dips like in Fig. 1(c) [Fig. 3(b)], giving the ground-state spectrum. From this signal we can determine N. With increasing V_{amp}, the dip widens [Fig. 3(c)]. A stepwise drop of g due to the first-excited orbital also appears. Application of magnetic field parallel to the 2DEG causes the Zeeman splitting of spin states, which is detected by the drop of g [Fig. 3(d)]. Note that in this measurement the one-dimensional bands in QW are also split by the Zeeman effect but E_F is placed far from the band edges and the difference between $D_\uparrow$ and $D_\downarrow$ can be ignored.

Now let us turn to the spin-polarization detection. Ideally the conductance of QW under zero magnetic field is quantized in units of $2e^2/h$, where the factor 2 originates from Kramers degeneracy. This produces staircaselike variation in the conductance through QW G_W versus the width of QW controlled by the wire gate voltage V_W.[19] Application of the parallel magnetic field lifts the Kramers degeneracy and conductance plateaus at odd multiples of e^2/h appear.[20,21] On such intermediate conductance plateaus, E_F lies between the two Zeeman-separated edges of one-dimensional bands; therefore, $D_\uparrow$ and $D_\downarrow$ are different. For example, at the lowest conductance plateau, only an up-spin band is occupied (P=1). The difference becomes very small on the conductance plateaus with even multiples of e^2/h. Hence P oscillates against V_W.

To detect P in QW, we apply the third method described in Sec. II. Figure 4 shows measured g as a function of V_{Pc} with changing V_W at 14 T. The upper trace is shifted by 0.7 for clarity. A two-step dip structure like in Fig. 2(c) is observed in the case of V_W=−0.375 V. But with V_W=−0.225 V, the trace is single step and indicates P=1. In this measurement, the change in Γ_1 with the shift of V_W is compensated by the readjustment of the coupling gate voltage V_C.

In Fig. 5(a), we plot G_W as a function of V_W. Short conductance plateaus (marked with open triangles) and long plateaus (solid triangles) are observed alternately. The short and

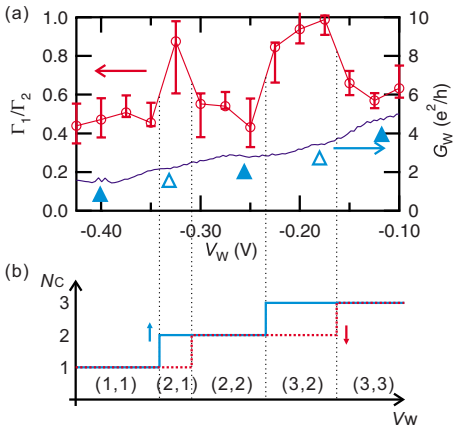

FIG. 5. (Color online) (a) Γ_1/Γ_2 (open circles) and G_W (lower solid trace) as functions of V_W. Open and solid triangles indicate the positions of odd and even plateaus, respectively. Error bars of Γ_1/Γ_2 arise from the uncertainties in evaluating Δg. (b) Estimated N_C for up (solid trace) and down (dotted trace) spins as a function of V_W. $(N_{C\uparrow},N_{C\downarrow})$ are indicated at the lower part of the figure.

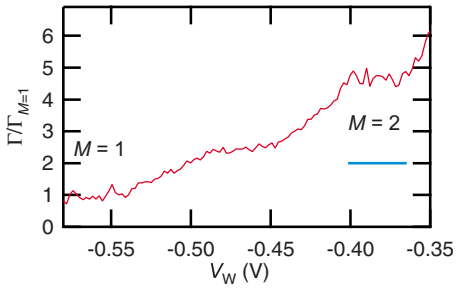

FIG. 6. (Color online) Measured $\Gamma/\Gamma_{M=1}$ as a function of V_W at zero magnetic field. The horizontal line around $V_W=-0.38$ V shows the estimated $\Gamma/\Gamma_{M=1}$ assuming $M=1$ and 2 channels have the same coupling strength.

long plateaus correspond to odd $(N_{C\uparrow}+N_{C\downarrow}=2n+1)$ and even $(N_{C\uparrow}+N_{C\downarrow}=2n)$ plateaus because the Zeeman splitting is smaller than the spacing between one-dimensional bands. Here, $N_{C\uparrow}$ and $N_{C\downarrow}$ are the number of channels with up and down spins, respectively, and n is a non-negative integer. The estimated N_C is shown in Fig. 5(b). In this device, the value of G_W at plateaus are not the multiples of e^2/h due primarily to the complexity of the gate configuration.

In Fig. 5(a), the values of Γ_1/Γ_2 obtained from the measured $\Delta g_1/\Delta g_2$ are shown with open circles. Near the even plateaus of G_W, Γ_1/Γ_2 is around 0.5 indicating P is almost zero. On the other hand, around the odd plateaus, Γ_1/Γ_2 goes up to 0.9 or 1.0 showing $P\approx 1$. This behavior is qualitatively in accordance with what is expected. These results certify that the system is working as a spin-polarization detector. Nevertheless, two puzzling points remain: (1) the region with large Γ_1/Γ_2 at $(N_{C\uparrow},N_{C\downarrow})=(3,2)$ is significantly wider than the width of the conductance plateau and (2) Γ_1/Γ_2 goes up to 1 even at higher plateau. If all of the channels have the same contribution on P, P is represented by $(N_{C\uparrow}-N_{C\downarrow})/(N_{C\uparrow}+N_{C\downarrow})\leq 1/(N_{C\uparrow}+N_{C\downarrow})$. Hence P should decrease with increasing N_C.

As for puzzle (1), the reason will be the spatial difference between the positions at which G_W is determined and the one at which QD couples to QW. Because QW in the present experiment is comparatively short, the electron wave function should be inevitably inhomogeneous along QW. G_W is determined by the narrowest part of QW while QD detects P at the connection point to QW. The two points are not necessarily same. Lowering of the band edge of higher channel down to E_F may occur at the QD-QW contact before the high channel opens at the narrowest point. This makes the difference between Γ_1/Γ_2 and G_W around the condition on which a new channel opens.

As for puzzle (2), the larger coupling strength between QD and QW for the higher channel will be the reason. To confirm this point, we check the change in Γ when a new channel in QW opens. Figure 6 shows the result. The measurement is performed in a device with the same design at zero magnetic field. Γ is normalized by the tunneling rate of the lowest channel $\Gamma_{M=1}$, where M is an index for channels. Steep increases in Γ are observed around $V_W=-0.51$ and -0.42 V which correspond to the beginning points of the ejection and injection with $M=2$ channel, respectively. If $M=1$ and 2 channels have the same coupling strength, $\Gamma/\Gamma_{M=1}$ becomes 2 when both channels open around $V_W=-0.38$ V as indicated with a horizontal line in Fig. 6. But the observed result is apparently larger than this line and shows that the higher channel has larger coupling. This originates from the shape of the wave function across QW. In the higher channel, the wave function of QW is extended to outer side and has larger overlap with the wave function of QD.

In the last part, we emphasize the small detection current needed in this detection scheme. The net current through QD during the measurement is apparently zero. The "exchange current" between the target and QD, defined as $=e/2\tau$, is also extremely small. In the detection in high magnetic field, we use $\tau\sim 1$ ms. Then the exchange current is about 100 aA. For the detection at zero magnetic field, because T_1 is on the order of ms,[22,23] τ should be smaller by 1 order or more. The exchange current in this case is $1\sim 10$ fA but still 2 orders of magnitude smaller than the current for ordinary conductance measurements. From these, we expect the proposed detector is promising for sensing spin polarization created in delicate mechanisms such as spin filtering by spin-orbit interaction, spin-Hall effect, etc.

In summary, we proposed realistic methods to detect local spin polarization by using a quantum dot side coupled to a target device. With a quantum wire in magnetic fields as a controllable spin-polarized source, we demonstrated the operation of the polarization detector experimentally. In the case of a quantum wire, we found that the dot selectively senses polarization of electrons in a channel which has largest coupling to the dot.

ACKNOWLEDGMENTS

We thank Y. Hashimoto for technical supports. This work was supported by Grant-in-Aid for Scientific Research and Special Coordination Funds for Promoting Science and Technology.

*t-otsuka@issp.u-tokyo.ac.jp

[1] S. A. Wolf, D. D. Awschalom, R. A. Buhrman, J. M. Daughton, S. von Molnár, M. L. Roukes, A. Y. Chtchelkanova, and D. M. Treger, Science **294**, 1488 (2001).
[2] I. Žutić, J. Fabian, and S. Das Sarma, Rev. Mod. Phys. **76**, 323 (2004).
[3] E. I. Rashba, Sov. Phys. Solid State **2**, 1109 (1960).
[4] Y. A. Bychkov and E. I. Rashba, J. Phys. C **17**, 6039 (1984).
[5] G. Dresselhaus, Phys. Rev. **100**, 580 (1955).
[6] A. A. Kiselev and K. W. Kim, Appl. Phys. Lett. **78**, 775 (2001).
[7] T. P. Pareek, Phys. Rev. Lett. **92**, 076601 (2004).
[8] M. Eto, T. Hayashi, and Y. Kurotani, J. Phys. Soc. Jpn. **74**, 1934 (2005).
[9] J. Ohe, M. Yamamoto, T. Ohtsuki, and J. Nitta, Phys. Rev. B **72**, 041308(R) (2005).
[10] G. Schmidt, D. Ferrand, L. W. Molenkamp, A. T. Filip, and B. J. van Wees, Phys. Rev. B **62**, R4790 (2000).
[11] S. Murakami, Adv. Solid State Phys. **45**, 197 (2005).
[12] J. Schliemann, Int. J. Mod. Phys. B **20**, 1015 (2006).
[13] M. Field, C. G. Smith, M. Pepper, D. A. Ritchie, J. E. F. Frost, G. A. C. Jones, and D. G. Hasko, Phys. Rev. Lett. **70**, 1311 (1993).
[14] E. Buks, R. Schuster, M. Heiblum, D. Mahalu, and V. Umansky, Nature (London) **391**, 871 (1998).
[15] J. M. Elzerman, R. Hanson, J. S. Greidanus, L. H. Willems van Beveren, S. De Franceschi, L. M. K. Vandersypen, S. Tarucha, and L. P. Kouwenhoven, Phys. Rev. B **67**, 161308(R) (2003).
[16] J. M. Elzerman, R. Hanson, L. H. Willems van Beveren, L. M. K. Vandersypen, and L. P. Kouwenhoven, Appl. Phys. Lett. **84**, 4617 (2004).
[17] T. Otsuka, E. Abe, Y. Iye, and S. Katsumoto, Appl. Phys. Lett. **93**, 112111 (2008).
[18] A. Aharony, O. Entin-Wohlman, Y. Tokura, and S. Katsumoto, Phys. Rev. B **78**, 125328 (2008).
[19] B. J. van Wees, H. van Houten, C. W. J. Beenakker, J. G. Williamson, L. P. Kouwenhoven, D. van der Marel, and C. T. Foxon, Phys. Rev. Lett. **60**, 848 (1988).
[20] B. J. van Wees, L. P. Kouwenhoven, H. van Houten, C. W. J. Beenakker, J. E. Mooij, C. T. Foxon, and J. J. Harris, Phys. Rev. B **38**, 3625 (1988).
[21] D. A. Wharam, T. J. Thornton, R. Newbury, M. Pepper, H. Ahmed, J. E. F. Frost, D. G. Hasko, D. C. Peacock, D. A. Ritchie, and G. A. C. Jones, J. Phys. C **21**, L209 (1988).
[22] R. Hanson, B. Witkamp, L. M. K. Vandersypen, L. H. Willems van Beveren, J. M. Elzerman, and L. P. Kouwenhoven, Phys. Rev. Lett. **91**, 196802 (2003).
[23] J. M. Elzerman, R. Hanson, L. H. Willems van Beveren, B. Witkamp, L. M. K. Vandersypen, and L. P. Kouwenhoven, Nature (London) **430**, 431 (2004).